We are IntechOpen, the world's leading publisher of Open Access books Built by scientists, for scientists

4,800
Open access books available

122,000
International authors and editors

135M
Downloads

Our authors are among the

154
Countries delivered to

TOP 1%
most cited scientists

12.2%
Contributors from top 500 universities

CLARIVATE ANALYTICS BOOK CITATION INDEX INDEXED

WEB OF SCIENCE™

Selection of our books indexed in the Book Citation Index in Web of Science™ Core Collection (BKCI)

Interested in publishing with us?
Contact book.department@intechopen.com

Numbers displayed above are based on latest data collected.
For more information visit www.intechopen.com

16

Enhancing Ultrasound Images Using Hybrid FIR Structures

L. J. Morales-Mendoza, Yu. S. Shmaliy and O. G. Ibarra-Manzano
Electronics Department, Guanajuato University
México

1. Introduction

The problem of saving a sharp edge with a simultaneous enhancing in the image is typical for ultrasound applications. Ultrasound imaging is a technique that is widely used in a variety of clinical applications, such as cardiology (Najarian & Splinter, 2007), obstetrics and gynecology (Jan, 2006), and others. Due to the blur and typically non Gaussian noise, an origin ultrasound image has a poor resolution. That forces researches to create image processing algorithms having a contradictive ability of cleaning the image of noise but saving its sharp edge. An overall panorama of nonlinear filtering following the median strategy has been presented by Pitas and Venetsanopoulos (Pitas & Venetsanopoulos, 1990) along with important modifications for a large class of nonlinear filters employing the order statistics. The algorithm issues for the filter design have been discussed in (Kalouptsidis & Theodoridis, 1993). In (Astola & Kuosmanen, 1997), the finite impulse response (FIR) median hybrid filters (MHF) strategy has been proposed with applications to image processing. An important step ahead has been made in (Heinonen & Neuvo, 1987; 1988), where the FIR MHF structures have been designed. In the sequel, the MHF structures have extensively been investigated, developed, and used by many authors.

Basically, hybrid FIR structures can be designed using different types of estimators. Among possible solutions, the polynomial estimators occupy a special place, since the polynomial models often well formalize a priori knowledge about different processes. Relevant signals are typically represented with degree polynomials to fit a variety of practical needs. Examples of applications of polynomial structures can be found in signal processing (Dumitrescu, 2007; Mathews & Sicuranza, 2001), timescales and clock synchronization (Shmaliy, 2006), image processing (Bose, 2004), speech processing (Heinonen & Neuvo, 1988), etc. The polynomial estimators suitable for such structures can be obtained from the generic form of the p-step predictive unbiased FIR filter proposed in (Shmaliy, 2006; 2009). Such estimators usually process data on finite horizons of N points that typically obtain a nice restoration.

In this Chapter, we first give the theory of the p-step smoothing unbiased FIR estimator of polynomial signals viewing an image as a multistate space model. We then use the polynomial solutions in the design of FIR MHF structures and justify optimal steps p from the standpoint of minimum produced errors. We show advantages of the approach employing the three generic ramp FIR solutions. Namely, we exploit the 1-step predictive

Source: Image Processing, Book edited by: Yung-Sheng Chen,
ISBN 978-953-307-026-1, pp. 572, December 2009, INTECH, Croatia, downloaded from SCIYO.COM

filter (p = 1), the filter (p = 0), and the 1-lag smoothing filter (p = -1). The hybrid structures investigated are compared in terms of the root mean square errors (RMSEs) and the signal-to-noise ratio (SNR) in the enhanced image. The rest of the chapter is organized as follows: In section II, we describe the polynomial image. In section III, the gains for the optimal and unbiased smoothing FIR filters are derived. The low-degree polynomials gains for unbiased smoothing FIR filters are considered in detain in section IV. Section V is defined to design and applications of unbiased FMH structures. Finally, the concluding remarks are drawn in section VI.

2. Polynomial image model

A two-dimensional image is often represented as a $k_c \times k_r$ matrix $\mathbf{M} = \{\mu_{i,j}\}$. To provide two dimensional filtering, the matrix can be written in the form of a row-ordered vector or a column-ordered vector, respectively,

$$\mathbf{x}_r = \left[\mu_{1,1}\mu_{1,2}\cdots\mu_{1,k_r}\mu_{2,1}\mu_{2,2}\cdots\mu_{2,k_r}\cdots\mu_{k_c,1}\mu_{k_c,2}\cdots\mu_{k_c,k_r}\right]^T, \tag{1}$$

$$\mathbf{x}_c = \left[\mu_{1,1}\mu_{2,1}\cdots\mu_{k_c,1}\mu_{1,2}\mu_{2,2}\cdots\mu_{k_c,2}\cdots\mu_{1,k_r}\mu_{2,k_r}\cdots\mu_{k_c,k_r}\right]^T. \tag{2}$$

The filtering procedure is then often applied twice, first to (1) and then to (2), or vice versa.
If to represent a two-dimensional electronic image with (1) and (2), then one may also substitute each of the vectors with the discrete time-invariant deterministic signal x_{1n} that, in turn, can be modeled on a horizon of some N points in state space. If x_{1n} projects ahead from $n - N + 1 - p$ to $n - p$, then the p-lag smoothing FIR filtering estimate can be provided at a current point n with a lag p, $p < 0$, as shown in Fig. 1. Referring to Fig. 1, a signal x_{1n} can further be projected on a horizon of N points from $n - N + 1 - p$, to n with the finite order Taylor series as follows:

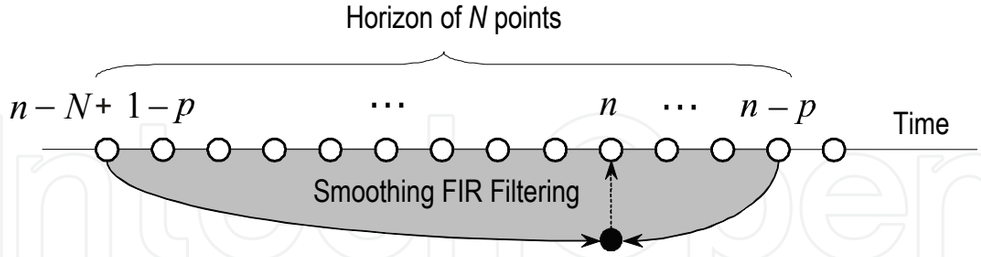

Fig. 1. Smoothing FIR filtering on a horizon of N points with a lag p, $p < 0$.

$$x_{1n} = \sum_{q=0}^{K-1} x_{(q+1)(n-N+1-p)} \frac{\tau^q (N-1+p)^q}{q!}$$

$$= x_{1(n-N+1-p)} + x_{2(n-N+1-p)}\tau(N-1+p) + x_{3(n-N+1-p)}\tfrac{1}{2}\tau^2(N-1+p)^2 +$$

$$\cdots + x_{K(n-N+1-p)}\tfrac{1}{(K-1)!}\tau^{K-1}(N-1+p)^{K-1}, \tag{3}$$

where $x_{(q+1)(n-N+1-p)}$, $q \in [0, K-1]$, can be called the signal $(q+1)$-state at $n-N+1-p$ and the signal thus characterized with K states, from 1 to K. Here, τ is the sampling time.
In such a model, the k-state, $k \in [1, K]$, is determined by the time derivative of the $(k-1)$-state, starting with $k = 2$. Therefore, most generally, we have

$$x_{kn} = \sum_{q=0}^{K-k} x_{(q+k)(n-N+1-p)} \frac{\tau^q (N-1+p)^q}{q!}$$

$$= x_{k(n-N+1-p)} + x_{(k+1)(n-N+1-p)} \tau (N-1+p) + x_{(k+2)(n-N+1-p)} \tfrac{1}{2} \tau^2 (N-1+p)^2 +$$

$$\cdots + x_{K(n-N+1-p)} \tfrac{1}{(K-k)!} \tau^{K-k} (N-1+p)^{K-k}. \quad (4)$$

If we now suppose that x_{1n} (1) is contaminated in the measurement to be s_n with noise v_n having zero mean $E\{v_n\} = 0$, and arbitrary distribution and covariance $\mathbf{Q} = E\{v_i v_j\}$, then the model and the measurement can be represented in state space, using (4), with the state and observation equations as, respectively

$$\mathbf{x}_n = \mathbf{A}^{N-1+p} \mathbf{x}_{n-N+1-p}, \quad (5)$$

$$s_n = \mathbf{C}\mathbf{x}_n + v_n, \quad (6)$$

where the $K \times 1$ state vector is given by

$$\mathbf{x}_n = \begin{bmatrix} x_{1n} & x_{2n} & \cdots & x_{Kn} \end{bmatrix}^T. \quad (7)$$

The $K \times K$ triangular matrix $\mathbf{A}^i$, projecting the state at $n-N+1-p$ to the present state at n, is specified with

$$\mathbf{A}^i = \begin{bmatrix} 1 & \tau i & \frac{1}{2}(\tau i)^2 & \cdots & \frac{1}{(K-1)!}(\tau i)^{K-1} \\ 0 & 1 & \tau i & \cdots & \frac{1}{(K-2)!}(\tau i)^{K-2} \\ 0 & 0 & 1 & \cdots & \frac{1}{(K-3)}(\tau i)^{K-3} \\ \vdots & \vdots & \vdots & \ddots & \vdots \\ 0 & 0 & 0 & \cdots & 1 \end{bmatrix}, \quad (8)$$

and the $1 \times K$ measurement matrix is

$$\mathbf{C} = \begin{bmatrix} 1 & 0 & \cdots & 0 \end{bmatrix}. \quad (9)$$

If we now think that the state space model (5) and (6) represents an electronic image, then we would like to find the optimal and unbiased gains for the smoothing FIR filter producing at n the estimate $\hat{\mathbf{x}}_{n|n-p}$, $p < 0$, associated with the enhanced image.

3. Smoothing FIR filtering of polynomial models

In FIR filtering, an estimate is obtained via the discrete convolution applied to measurement. That can be done if to represent the state space model on an averaging interval of some N points as shown in (Shmaliy, 2008). Referring to Fig. 1, we thus can represent the model (3) and (4) on a horizon from $n - N + 1 - p$ to $n - p$. The recursively computed forward-in-time solutions given us

$$\mathbf{X}_N(p) = \mathbf{A}_N \mathbf{x}_{n-N+1-p}, \tag{10}$$

$$\mathbf{S}_N(p) = \mathbf{C}_N \mathbf{x}_{n-N+1-p} + \mathbf{V}_N(p), \tag{11}$$

where

$$\mathbf{X}_{N(p)} = \begin{bmatrix} \mathbf{x}_{n-p}^T & \mathbf{x}_{n-1-p}^T & \cdots & \mathbf{x}_{n-N+1-p}^T \end{bmatrix}^T, \tag{12}$$

$$\mathbf{S}_N(p) = \begin{bmatrix} s_{n-p} & s_{n-1-p} & \cdots & s_{n-N+1-p} \end{bmatrix}^T, \tag{13}$$

$$\mathbf{V}_N(p) = \begin{bmatrix} v_{n-p} & v_{n-1-p} & \cdots & v_{n-N+1-p} \end{bmatrix}^T, \tag{14}$$

$$\mathbf{A}_N = \begin{bmatrix} (\mathbf{A}^{N-1+p})^T & (\mathbf{A}^{N-2+p})^T & \cdots & (\mathbf{A}^{1+p})^T & (\mathbf{A}^{p})^T \end{bmatrix}^T, \tag{15}$$

$$\mathbf{C}_N = \begin{bmatrix} \mathbf{C}\mathbf{A}^{N-1+p} \\ \mathbf{C}\mathbf{A}^{N-2+p} \\ \vdots \\ \mathbf{C}\mathbf{A}^{1+p} \\ \mathbf{C}\mathbf{A}^{p} \end{bmatrix} = \begin{bmatrix} (\mathbf{A}^{N-1+p})_1 \\ (\mathbf{A}^{N-2+p})_1 \\ \vdots \\ (\mathbf{A}^{1+p})_1 \\ (\mathbf{A}^{p})_1 \end{bmatrix}, \tag{16}$$

where $(\mathbf{Z})_1$ means the first row of a matrix $\mathbf{Z}$. Given (10) and (11), the smoothing FIR filtering estimate is obtained as in the following.

It is known that FIR estimates can be found for each of the states separately. Following this line and utilizing N measurements from $n - N + 1 - p$ to $n - p$, the smoothing FIR filtering estimate $\hat{x}_{1n|n-p}$ of x_{1n} can be obtained at n as

$$\hat{x}_{1n|n-p} = \sum_{i=p}^{N-1+p} h_{li}(p) y_{n-i}, \tag{17a}$$

$$= \mathbf{W}_l^T(p) \mathbf{S}_N, \tag{17b}$$

$$= \mathbf{W}_l^T(p) \left[\mathbf{C}_N \mathbf{x}_{n-N+1-p} + \mathbf{V}_N(p) \right], \tag{17c}$$

where $h_{li}(p) \equiv h_{li}(N, p)$ is the l-degree filter gain (Shmaliy, 2006) dependent on N and p and the l-degree and $1 \times N$ filter gain matrix is given with

$$\mathbf{W}_l^T(p) = \begin{bmatrix} h_{lp}(p) & h_{l(1+p)}(p) & \cdots & h_{l(N-1+p)}(p) \end{bmatrix}. \tag{18}$$

Note that $h_{li}(p)$ in (17a) and (18) can be specified in different sense depending on applications. Below, we investigate this gain in the sense of the minimum bias in order to design the hybrid FIR filters.

3.1 Unbiased estimate

The unbiased smoothing FIR filtering estimates can be found if we start with the unbiasedness condition

$$E\{\hat{x}_{1n|n-p}\} = E\{x_{1n}\} \tag{19}$$

substitute x_{1n} with

$$x_{1n} = \left(\mathbf{A}^{N-1+p}\right)_1 \mathbf{x}_{n-N+1-p} \tag{20}$$

and $\hat{x}_{1n|n-p}$ with (17c). That leads to the unbiasedness (or deadbeat) constraint

$$\left(\mathbf{A}^{N-1+p}\right)_1 = \overline{\mathbf{W}}_l^T(p)\mathbf{C}_N, \tag{21}$$

where $\overline{\mathbf{W}}_l(p)$ mean the l-degree unbiased gain matrix (Shmaliy, 2006).

It can be show that the constraint (21) does not give us a direct solution for the gain matrix. Instead, one can equate the components of the row matrices in (21) and, similarly to (Shmaliy, Apr. 2009), arrive at

$$1 = \sum_{i=p}^{N-1+p} h_{li}(p)$$

$$\tau(N-1+p) = \sum_{i=p}^{N-1+p} h_{li}(p)\tau(N-1-i+p) + \sum_{i=p}^{N-1+p} h_{li}(p)$$

$$\vdots$$

$$\frac{\left[\tau(N-1+p)\right]^{K-1}}{(K-1)!} = \sum_{i=p}^{N-1+p} h_{li}(p)\frac{\left[\tau(N-1-i+p)\right]^{K-1}}{(K-1)!}$$

$$+\cdots+ \sum_{i=p}^{N-1+p} h_{li}(p)\tau(N-1-i+p) + \sum_{i=p}^{N-1+p} h_{li}(p). \tag{22}$$

Further accounting the first identity in the remaining ones of (22) leads to the fundamental properties of the p-lag unbiased smoothing FIR filter gain:

$$\sum_{i=p}^{N-1+p} h_{li}(p) = 1$$

$$\sum_{i=p}^{N-1+p} h_{li}(p) i^u = 0, \quad 1 \le u \le l. \tag{23}$$

A short matrix form (23) is thus

$$\overline{\mathbf{W}}_l^T(p)\mathbf{V}(p) = \mathbf{J}^T, \tag{24}$$

where

$$\mathbf{J} = \left[\underbrace{1 \quad 0 \quad \cdots \quad 0}_{N}\right]^T \tag{25}$$

and the p-lag and $N \times (l + 1)$ Vandermonde matrix is specified by

$$\mathbf{V}(p) = \begin{bmatrix} 1 & p & p^2 \\ 1 & 1+p & (1+p)^2 \\ 1 & 2+p & (2+p)^2 \\ \vdots & \vdots & \vdots \\ 1 & N-1+p & (N-1+p)^2 \end{bmatrix}. \tag{26}$$

Now note that the inverse $\left[\mathbf{V}^T(p)\mathbf{V}(p)\right]^{-1}$ always exists. Then multiply the right-side of (24) with the identity matrix $\left[\mathbf{V}^T(p)\mathbf{V}(p)\right]^{-1}\mathbf{V}^T(p)\mathbf{V}(p)$, discard $\mathbf{V}(p)$ from the both sides, and finally arrive at the fundamental solution for the gain,

$$\overline{\mathbf{W}}_l^T(p) = \mathbf{J}^T\left[\mathbf{V}^T(p)\mathbf{V}(p)\right]^{-1}\mathbf{V}(p) \tag{27}$$

that can be used for unbiased FIR filtering of polynomial models. Because no restriction is imposed upon p, the gain (27) can be used for FIR filtering with $p = 0$, smoothing FIR filtering with $p < 0$, and predictive FIR filtering with $p > 0$.

3.2 Unbiased polynomial gain

Although (27) is an exact and simple solution for unbiased FIR estimation, there is an inconvenience in using the Vandermonde matrix acquiring large dimension when N is large. On the other hand, we still have no idea about the gain function $h_{li}(p)$. To find this function, the following fundamental property can be invoked from the Kalman-Bucy filter theory: the order of the optimal (and unbiased) filter is the same as that of the system. This property suggests that the *kth* state of the model characterized with K states can unbiasedly be filtered with the $l = K - k$ degree FIR filter (Shmaliy, 2006). In other words: the first state x_{kn}, $k = 1$, of

the K-state model can unbiasedly be filtered, smoothed, and predicted with the gain of degree $l = K - 1$.
Most generally, following (Shmaliy, 2006), we thus can represent the filter gain with the degree polynomial

$$h_{li}(p) = \sum_{j=0}^{l} a_{jl}(p) i^j , \tag{28}$$

where $l \in [1, K]$, $i \in [p, N - 1 + p]$, and $a_{jl}(p) \equiv a_{jl}(N, p)$ is still unknown coefficient.
Substituting (28) to (27) and rearranging the terms lead to a set linear equations, having a compact matrix form of

$$\mathbf{J} = \mathbf{D}(p)\boldsymbol{\gamma}(p), \tag{29}$$

where

$$\mathbf{J} = \left[\underbrace{1 \quad 0 \quad \cdots \quad 0}_{K} \right]^T , \tag{30}$$

$$\boldsymbol{\gamma} = \left[\underbrace{a_{0(K-1)} \quad a_{1(K-1)} \quad \cdots \quad a_{(K-1)(K-1)}}_{K} \right]^T , \tag{31}$$

and a short symmetric $l \times l$ matrix $\mathbf{D}(p)$ is specified via the Vandermonde matrix (26) as

$$\mathbf{D}(p) = \mathbf{V}^T(p)\mathbf{V}(p)$$

$$= \begin{bmatrix} d_0(p) & d_1(p) & \cdots & d_l(p) \\ d_1(p) & d_2(p) & \cdots & d_{l+1}(p) \\ \vdots & \vdots & \ddots & \vdots \\ d_l(p) & d_{l+1}(p) & \cdots & d_{2l}(p) \end{bmatrix}. \tag{32}$$

The component for (32) is defined by

$$d_m(p) = \sum_{i=p}^{N-1+p} i^m , \; m = 0,1 \ldots 2l , \tag{33}$$

$$= \frac{1}{m+1}\left[B_{m+1}(N + p) - B_{m+1}(p) \right], \tag{34}$$

where $B_n(x)$ is the Bernoulli polynomial.

An analytic solution to (29), with respect to the coefficients $a_{jl}(p)$ of the polynomial (28), gives us

$$a_{jl}(p) = (-1)^j \frac{M_{(j+1)1}(p)}{|\mathbf{D}|}, \tag{35}$$

where $|\mathbf{D}|$ is the determinant of $\mathbf{D}(p)$ that turns out to be p-invariant, and $M_{(j+1)1}(p)$ is the minor of $\mathbf{D}(p)$.

Determined $a_{jl}(p)$ and $h_{li}(p)$, the unbiased smoothing FIR filter of the polynomial signal x_{1n} is provided as follows. Given a discrete time-invariant polynomial state space model, (5) and (6), then the p-lag unbiased smoothing FIR filtering estimate of the model x_{1n} having K states is obtained at n on a horizon of N points using the data s_n taken from $n - N + 1 - p$ to $n - p$, $p < 0$, by

$$\hat{x}_{1n|n-p} = \sum_{i=p}^{N-1+p} h_{(K+1)i}(p) s_{n-i}, \tag{36}$$

$$= \overline{\mathbf{W}}_l^T(p) \mathbf{S}_N, \tag{37}$$

where $\overline{\mathbf{W}}_l(p)$ is specified with (18), $h_{li}(p)$ with (28) and (35), and $\mathbf{S}_N$ is the data vector (13).

3.2.3 Properties of the polynomial gain

The l-degree and p-lag polynomial gain $h_{li}(p)$ has the following fundamental properties:

- Its range of existence is

$$h_{li}(p) = \begin{cases} h_{li}(p) & p \le N-1+p \\ 0 & \text{otherwise} \end{cases}. \tag{38}$$

- The gain has unit area and zero moments as follows, respectively,

$$\sum_{i=p}^{N-1+p} h_{li}(p) = 1, \tag{39}$$

$$\sum_{i=p}^{N-1+p} h_{li}(p) i^u = 0, \; 1 \le u \le l. \tag{40}$$

- Its energy, referring to (39) and (40), calculates

$$\sum_{i=p}^{N-1+p} h_{li}^2(p) = \sum_{i=p}^{N-1+p} h_{li}(p) \sum_{j=0}^{l} a_{jl}(p) i^j$$

$$= \sum_{j=0}^{l} a_{jl}(p) \sum_{i=p}^{N-1+p} h_{li}(p) i^j$$

$$= a_{0l}(p), \tag{41}$$

where $a_{0l}(p)$ is the zero-order coefficient in (28).

3.3 Estimate variance

For the zero-mean measurement noise v_n having arbitrary distribution and covariance, the variance of the unbiased smoothing FIR filtering estimate can be found via the mean square error (MSE)

$$J = E(x_{1n} - \hat{x}_{1n|n-p})^2$$
$$= E\left[x_{1n} - \overline{\mathbf{W}}_l^T(p)\mathbf{C}_N\mathbf{x}_{n-N+1-p} - \overline{\mathbf{W}}_l^T(p)\mathbf{V}_N(p)\right]^2$$

$$= E\left[\left(\mathbf{A}^{N-1+p}\right)_1\mathbf{x}_{n-N+1-p} - \overline{\mathbf{W}}_l^T(p)\mathbf{C}_N\mathbf{x}_{n-N+1-p} - \overline{\mathbf{W}}_l^T(p)\mathbf{V}_N(p)\right]^2. \tag{42}$$

Embedded the unbiasedness (21) and accounted for the commutativity $\overline{\mathbf{W}}_l^T\mathbf{V}_N = \mathbf{V}_N^T\overline{\mathbf{W}}_l$, the MSE (42) represents the variance

$$\sigma^2(p) = E\left[\overline{\mathbf{W}}_l^T(p)\mathbf{V}_N(p)\right]^2$$
$$= E\left[\overline{\mathbf{W}}_l^T(p)\mathbf{V}_N(p)\overline{\mathbf{W}}_l^T(p)\mathbf{V}_N(p)\right] = \overline{\mathbf{W}}_l^T(p)E\left[\mathbf{V}_N(p)\mathbf{V}_N^T(p)\right]\overline{\mathbf{W}}_l(p)$$

$$= \overline{\mathbf{W}}_l^T(p)\mathbf{\Phi}_{\mathbf{V}}(p)\overline{\mathbf{W}}_l(p). \tag{43}$$

In an important special case when v_n is a white sequence having a constant variance σ_v^2, (43) becomes

$$\sigma^2(p) = \overline{\mathbf{W}}_l^T(p)\mathrm{diag}\left(\underbrace{\sigma_v^2 \quad \sigma_v^2 \quad \cdots \quad \sigma_v^2}_{N}\right)\overline{\mathbf{W}}_l(p) = \sigma_v^2 g_l(p), \tag{44}$$

where the noise power gain (NG) $g_l(p)$ is specified by (Heinonen & Neuvo, 1987)

$$g_l(p) = \overline{\mathbf{W}}_l^T(p)\overline{\mathbf{W}}_l(p) \tag{45a}$$

$$= \sum_{i=p}^{N-1+p} h_{li}^2(p) \tag{45b}$$

$$= a_{0l}(p). \tag{45c}$$

and states that reducing noise in the estimate, by diminishing $g_l(p)$, means reducing $a_{0l}(p)$.

4. Low degree polynomial gains for unbiased smoothing FIR filters

Typically, smoothing of images is provided on short horizons with low-degree polynomials. Below, we derive and investigate the relevant unique gains for the uniform, linear, quadratic and cubic models covering an overwhelming majority of practical needs.

4.1 Uniform model

A model that is uniform over an averaging horizon of N points is the simplest one. The relevant image is characterized with single state and the filter gain is represented, by (36), with the 0-degree polynomial as

$$h_{0i}(p) = h_{0i} = \begin{cases} \frac{1}{N} & p \le N - 1 + p \\ 0 & \text{otherwise} \end{cases}. \tag{46}$$

By (45c), the NG of this filter becomes p-invariant, namely $g_0(p) = g_0 = 1/N$. Because this gain is associated with simple averaging, it is also optimal for a common task (Smith, 1999): reducing random noise while retaining a sharp step response. No other filter is better than the simple moving average in this sense. However, this gain is not good in terms of the estimate bias that reaches 50% when the model behaves linearly. Therefore, the best smooth is obtained by this gain at a centre of the averaging horizon, namely when $p = -(N - 1)/2$.

4.2 Linear model

For linear models, the p-lag gain, existing from p to $N - 1 + p$, becomes ramp

$$h_{1i}(p) = a_{01}(p) + a_{11}(p)i, \tag{47}$$

having the coefficients

$$a_{01}(p) = \frac{2(2N-1)(N-1) + 12p(N-1+p)}{N(N^2-1)}, \tag{48}$$

$$a_{11}(p) = -\frac{6(N-1+2p)}{N(N^2-1)}. \tag{49}$$

At a centre of the averaging horizon provided with $p = -(N - 1)/2$, the ramp gain degenerates to the uniform one (46),

$$h_{1i}\left(N, -\frac{N-1}{2}\right) = g_1\left(N, -\frac{N-1}{2}\right) = h_{0i} = g_0 = \frac{1}{N}. \tag{50}$$

With this lag, the ramp gain (47) is thus optimal with its zero bias and minimum possible noise produced by simple averaging. It can be shown that an increase in $|p|$ from 0 to $(N - 1)/2$ results in reducing the ramp gain negative slope. As stated by (50), the lag $p = -(N - 1)/2$ can degenerate this gain to the uniform one (46) featured to simple averaging. Further increase in $|p|$ from $(N - 1)/2$ to $N - 1$ produces an opposite effect: the gain slope becomes positive and such that, with $p = -N + 1$, the gain function looks like symmetrically reflected from that corresponding to $p = 0$. Definitely, an ability of the ramp gain of becoming uniform with $p = -(N - 1)/2$ must affect the noise amount in the smooth. An investigation of the noise reduction can be provided using the NG

$$g_1(p) = a_{10}(p) = \frac{2(2N-1)(N-1) + 12p(N-1+p)}{N(N^2-1)}. \tag{51}$$

Instantly one realizes that noise in the smooth has lower intensity than in the filtering estimate ($p = 0$). Indeed, when p ranges as $-N + 1 < p < -(N - 1)/2$, the NG traces below the bound produced by $p = 0$. A situation changes when $|p|$ exceeds $N - 1$. With such values of the lag, the NG rises dramatically. One should not be surprised of this fact, because smoothing with lags exceeding and averaging horizon is nothing more than the backward prediction producing noise lager than in the filtering estimate.

4.3 Quadratic model

For the quadratic model, the gain of the unbiased smoothing FIR filter becomes

$$h_{2i}(p) = a_{02}(p) + a_{12}(p)i + a_{22}(p)i^2, \tag{52}$$

in which the coefficients are defined as

$$a_{02}(p) = 3\frac{\begin{array}{c}\left(3N^4 - 12N^3 + 17N^2 - 12N + 4\right) + 12(N-1)\left(2N^2 - 5N + 2\right)p \\ +12\left(7N^2 - 15N + 7\right)p^2 + 120(N-1)p^3 + 60p^4\end{array}}{N\left(N^2 - 1\right)\left(N^2 - 4\right)}, \tag{53}$$

$$a_{12}(p) = -18\frac{\begin{array}{c}\left(2N^3 - 7N^2 + 7N - 2\right) + 2\left(7N^2 - 15N + 7\right)p \\ +30(N-1)p^2 + 60p^4\end{array}}{N\left(N^2 - 1\right)\left(N^2 - 4\right)}, \tag{54}$$

$$a_{22}(p) = 30\frac{\left(N^2 - 3N + 2\right) + 6(N-1)p + 6p^2}{N\left(N^2 - 1\right)\left(N^2 - 4\right)}. \tag{55}$$

As well as the ramp gain (47), the quadratic one (52) has several special points. Namely, by the lags

$$p_{21} = -\frac{N-1}{2} + \sqrt{\frac{N^2 - 1}{12}}, \tag{56}$$

$$p_{22} = -\frac{N-1}{2} - \sqrt{\frac{N^2 - 1}{12}}, \tag{57}$$

this gain degenerates to the ramp one and, with $p = -(N - 1)/2$, it becomes symmetric. At the middle of the averaging horizon, $p = -(N - 1)/2$, the gain (52) simplifies to

$$h_{2i}\left(N, -\frac{N-1}{2}\right) = \frac{3}{4}\frac{3N^2 - 7 - 20i^2}{N\left(N^2 - 4\right)}. \tag{58}$$

The NG associated with the quadratic gain (52) is given by

$$g_2(p) = a_{02}(p), \tag{59}$$

where $a_{02}(p)$ is described with (53).

Unlike the p-lag ramp gain (47) having a lower bound for the NG at $1/N$, the relevant bound for the p-lag quadratic gain (52) ranges upper and is given by

$$g_{2\min} = \frac{3\left(3N^2-2\right)}{5N\left(N^2-1\right)}, \tag{60}$$

This value appears if to put to zero the derivative of $g_2(N, p)$ with respect to p and find the roots of the polynomial. Two lags correspond to (60), namely,

$$p_{23} = -\frac{N-1}{2} + \frac{1}{2}\sqrt{\frac{N^2+1}{5}}, \tag{61}$$

$$p_{24} = -\frac{N-1}{2} - \frac{1}{2}\sqrt{\frac{N^2+1}{5}}. \tag{62}$$

Like the ramp gain case, here noise in the smooth is lower than in the filtering estimate, if p does not exceed and averaging horizon. Otherwise, we watch for the increase in the error that can be substantial.

4.4 Cubic model

The p-lag cubic gain can now be derived in a similar manner to have a polynomial form of

$$h_{3i}(p) = a_{03}(p) + a_{13}(p)i + a_{23}(p)i^2 + a_{33}(p)i^3 \tag{63}$$

with the coefficients defines as

$$a_{03}(p) = 8\frac{\begin{array}{l}\left(2N^6-15N^5+47N^4-90N^3+113N^2-75N+18\right)\\+5\left(6N^5-42N^4+107N^3-132N^2+91N-30\right)p\\+5\left(42N^4-213N^3+378N^2-288N+91\right)p^2\\+10\left(71N^3-246N^2+271N-96\right)p^3\\+5\left(246N^2-525N+271\right)p^4+1050(N-1)p^5+350p^6\end{array}}{N\left(N^2-1\right)\left(N^2-4\right)\left(N^2-9\right)}, \tag{64}$$

$$a_{13}(p) = -20\frac{\begin{array}{l}\left(6N^5-42N^4+107N^3-132N^2+91N-30\right)\\+2\left(42N^4-213N^3+378N^2-288N+91\right)p\\+2\left(213N^3-738N^2+813N-288\right)p^2\\+4\left(246N^2-525N+271\right)p^3+1050(N-1)p^4+420p^5\end{array}}{N\left(N^2-1\right)\left(N^2-4\right)\left(N^2-9\right)}, \tag{65}$$

$$a_{23}(p)=120\frac{\begin{array}{c}\left(2N^4-13N^3+28N^2-23N+6\right)\\+2\left(13N^3-48N^2+58N-23\right)p\\+2\left(48N^2-105N+58\right)p^2+140(N-1)p^3+70p^4\end{array}}{N\left(N^2-1\right)\left(N^2-4\right)\left(N^2-9\right)},\tag{66}$$

$$a_{33}(p)=-140\frac{\begin{array}{c}\left(N^3-6N^2+11N-6\right)+2\left(6N^2-15N+11\right)p\\+30(N-1)p^2+20p^3\end{array}}{N\left(N^2-1\right)\left(N^2-4\right)\left(N^2-9\right)}.\tag{67}$$

As well as the ramp and quadratic gains, the cubic one demonstrates several important features, including an ability of converting to the quadratic gain. The special values of p associated with this gain are listed below

$$p_{31}=-\frac{N-1}{2}+\frac{1}{10}\sqrt{5\left(3N^2-7\right)},\tag{68}$$

$$p_{32}=-\frac{N-1}{2}+\frac{\sqrt{105}}{210}\sqrt{33N^2-17+2\sqrt{36N^4+507N^2-2579}},\tag{69}$$

$$p_{33}=-\frac{N-1}{2}+\frac{\sqrt{105}}{210}\sqrt{33N^2-17-2\sqrt{36N^4+507N^2-2579}},\tag{70}$$

$$p_{34}=-\frac{N-1}{2}-\frac{\sqrt{105}}{210}\sqrt{33N^2-17-2\sqrt{36N^4+507N^2-2579}},\tag{71}$$

$$p_{35}=-\frac{N-1}{2}-\frac{\sqrt{105}}{210}\sqrt{33N^2-17+2\sqrt{36N^4+507N^2-2579}},\tag{72}$$

$$p_{36}=-\frac{N-1}{2}-\frac{1}{10}\sqrt{5\left(3N^2-7\right)}.\tag{73}$$

The lags p_{31}, $p = -(N-1)/2$, and p_{36} convert the cubic gain to the quadratic one. These lags are therefore preferable from the standpoint of filtering accuracy, because the quadratic gain produces lower noise. The lag p_{32}, $p = -(N-1)/2$, and p_{35} correspond to minima on the smoother NG characteristic. The remaining lags, p_{33} and p_{34}, cause two maxima in the range of $-N+1 < p < 0$.

The NG corresponding to the cubic gain (63) is given by

$$g_3(p)=a_{03}(p).\tag{74}$$

where $a_{03}(p)$ is specified with (64). It can be shown that this NG ranges above the lower bound

$$g_{3\min} = \sqrt{\frac{3\left(3N^2 - 7\right)}{4N\left(N^2 - 4\right)}} \tag{75}$$

and, with p = const, it asymptotically approaches $g_3(N, 0)$, by increasing N. As well as in the quadratic gain case, noise in the cubic-gain smoother can be much lower than in the relevant filter ($p = 0$). On the other hand, the range of uncertainties is broadened here to $N = 3$ and the smoother becomes thus lower inefficient at short horizons. In fact, when the gain (74) exceeds unity, the 3-degree unbiased smoothing FIR filter loses an ability of denoising and its use becomes hence meaningless.

4.5 Generalizations

Several important common properties of the unbiased smoothing FIR filters can now be outlined as in the following. Effect of the lag p on the NG of low-degree unbiased smoothing FIR filters is reflected in Fig. 2. As can be seen, the NG of the ramp gain is exactly that of the uniform gain, when $p = -(N - 1)/2$. By $p = p_{21}$ and $p = p_{22}$, where p_{21} and p_{22} are specified by (61) and (62), respectively, the NG of the quadratic gain degenerates to that of the ramp gain. Also, by $p = p_{31}$ (68), $p = -(N - 1)/2$, and $p = p_{36}$ (73), the NG of the cubic gain degenerates to that of the quadratic gain. Similar deductions can be made for higher degree gains.

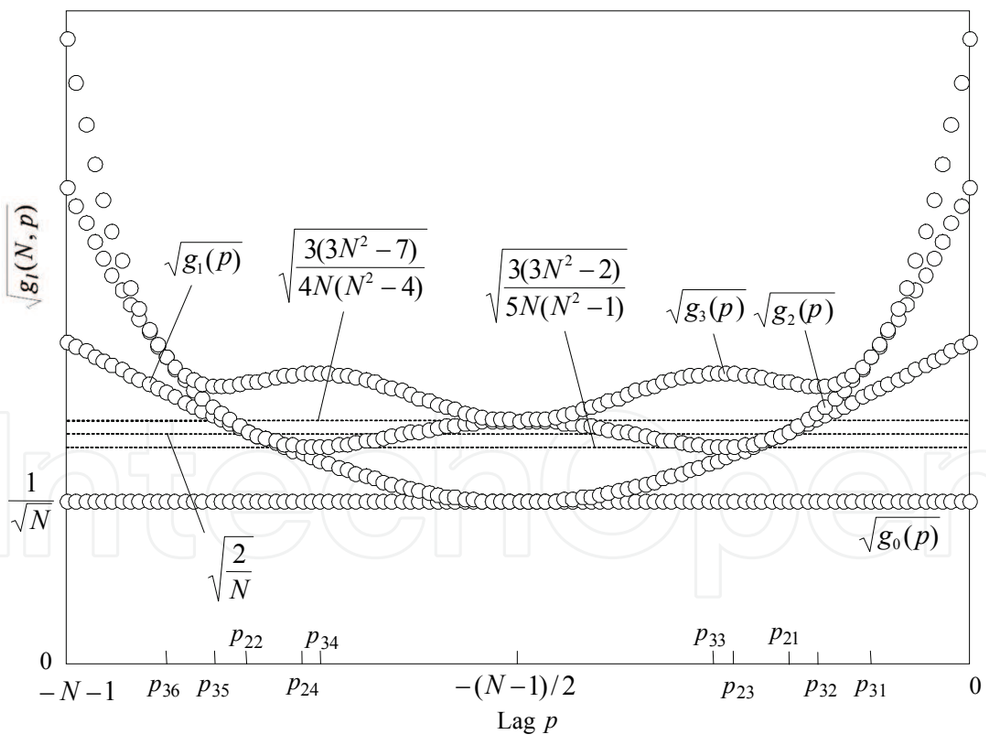

Fig. 2. Effect of a lag p, $p < 0$, on the NG of the low-degree unbiased smoothing FIR filters.

The following generalization can now be provided for a two-parameter family of the l-degree and p-lag, $p < 0$, unbiased smoothing FIR filters specified with the gain $h_{li}(p)$ and NG $g_l(p)$:

i. Any smoothing FIR filter with the lag p lying on the averaging horizon $-(N-1) < p < 0$, produces smaller errors then the relevant FIR filter with $p = 0$.
ii. Without loss in accuracy, the l-degree unbiased smoothing FIR filter can be substituted, for some special values of p, with a reduced $(l-1)$-degree one. Namely, the 1-degree gain can be substituted with the 0-degree gain for $p = -(N-1)/2$, the 2-degree gain with the 1-degree gain for $p = p_{21}$ and $p = p_{22}$, and the 3-degree gain with the 2-degree gain, if $p = p_{31}$, $p = -(N-1)/2$, or $p = p_{36}$.
iii. Beyond the averaging horizon, the error of the smoothing FIR filter with $p < -N+1$ is equal to that of the predictive FIR filter with $p > 0$.
iv. The error lower bounds for the smoothing FIR filters with the ramp gain, $g_{1\min}$, quadratic gain $g_{2\min}$, and cubic gain, $g_{3\min}$, are given by, respectively,

$$g_{1\min} = \frac{1}{N}, \tag{76}$$

$$g_{2\min} = \frac{3\left(3N^2-2\right)}{5N\left(N^2-1\right)}\bigg|_{N>>1} \approx \frac{9}{5N}, \tag{77}$$

$$g_{3\min} = \frac{3\left(3N^2-7\right)}{4N\left(N^2-4\right)}\bigg|_{N>>1} \approx \frac{9}{4N}, \tag{78}$$

v. With large N, error in the l-degree smoother for $p = -N+1$ are defined by

$$g_l\left(N,-N+1\right)\big|_{N>>1} \approx \frac{(l+1)^2}{N}. \tag{79}$$

The initial conditions can hence be ascertained using the ramp and quadratic gains with the NGs $\approx 4/N$ and $\approx 9/N$, respectively.
vi. By increasing N for a constant p such that $p << N$, the error in the smoother asymptotically approaches the error in the relevant unbiased FIR filter with $p = 0$.

5. Design and applications of unbiased FMH structures

In this section, we employ the above derived p-dependent gains in order to design efficient hybrid structures suitable for biomedical applications, specifically for ultrasound image processing. Every image is considered as an array of two signals, $\mathbf{x}_r$ and $\mathbf{x}_c$, as showed in (1) and (2), respectively, and processed as in the following. First, we filter out noise in the row vector and then reconstruct the image. Next, the partly enhanced image is decomposed to the column vector, the filtering procedure is applied once again, and the fully enhanced image is reconstructed. For the sake of minimum errors in the enhanced image, all of the above designed low-degree polynomial gains have been examined in the FMH structure. Namely, we employ all p-dependent, the ramp gain (47), the quadratic gain (52), and the cubic one (63). Two metrics, namely the signal-to-noise ratio (SNR) and the root mean square error (RMSE) have been used for the quantitative evaluation of the filter efficiency. It is known that FMH structures can be designed to have k substructures and that a number of

such substructures needs to be optimized that is a special topic. Postponing the optimization problem to further investigations, we mostly examine in this Chapter the basic FMH structure and demonstrate the effect of a number of sub-blocks.

5.1 Basic FIR median hybrid structure

Figure 3 sketches the block diagram of the basic FIR median hybrid (FMH) structure developed in (Heinonen & Neuvo, 1987) to maximize the SNR in the row and column vectors. Here, the input signal y_n is filtered with 2 FIR filters. The forward FIR filter (FIR^{FW}) computes the points on a horizon to the left from the point n. In turn, the backward FIR filter (FIR^{BW}) processes data on the same length horizon lying to the right from n. The estimates are hence formed as, respectively,

$$\hat{x}_n^{FW}(p) = \sum_{i=p}^{N-1+p} h_{li}(p) y_{n-i} \,, \tag{80}$$

$$\hat{x}_n^{BW}(p) = \sum_{i=p}^{N-1+p} h_{li}(p) y_{n+i} \,, \tag{81}$$

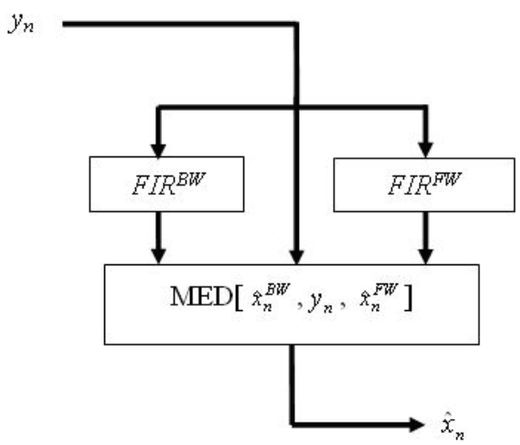

Fig. 3. Block diagram of the basic FIR median hybrid (FMH) structure.

The output signal $\hat{x}_n(p)$ is obtained using the nonlinear operator called the "median". In the median structure MED[$\hat{x}_n^{BW}(p)$, y_n, $\hat{x}_n^{FW}(p)$] (Fig. 3), the input y_n and the outputs of the FIR filters, $\hat{x}_n^{BW}(p)$ and $\hat{x}_n^{FW}(p)$, play the role of entries. Following the median filter strategy, the output $\hat{x}_n(p)$ becomes equal to the intermediate value that is stated by the operator

$$\hat{x}_n(p) = \mathrm{MED}\left[\hat{x}_n^{BW}(p), y_n, \hat{x}_n^{FW}(p)\right] \,. \tag{82}$$

Note that the best filtering result can be obtained if one sets properly the smoother lag p or prediction step p in the FIR filters. Because the basic structure shown in Fig. 3 is commonly unable to obtain nice image enhancing, owing to a small number of the entries, a more sophisticated FIR FMH structure exploiting different p would provide better performance.

In this Chapter, we employ the combined FIR FMH structure with $k > 1$ as shown in (Heinonen & Neuvo, 1987).

5.2 SNR and RMSE metrics

Image enhancement can quantitatively be evaluated using the SNR and RMSE metrics. Given the discrete image mapping $x_n(i,j)$, where $i \in [1,P]$ and $j \in [1,Q]$, and the relevant enhanced and reconstructed mapping $\hat{x}_n(i,j)$, the SNR can be estimated (in dB) by

$$SNR_{dB} = 10\log_{10}\left(\frac{\sum_{i=1}^{P}\sum_{j=1}^{Q}\left[x(i,j)\right]^2}{\sum_{i=1}^{P}\sum_{j=1}^{Q}\left[x(i,j)-\hat{x}(i,j)\right]^2}\right), \tag{83}$$

In turn, the RMSE in the enhanced image can be estimated with

$$RMSE = \sqrt{\frac{1}{PQ}\sum_{i=1}^{P}\sum_{j=1}^{Q}\left[x(i,j)-\hat{x}(i,j)\right]^2}\,. \tag{84}$$

Below, we apply these metrics to ultrasonic images.

5.3 Simulation and numerical evaluations

For further investigations, we chose a renal ultrasound image shown in Fig.4. This image has been obtained under the conditions accepted in (K. Singh & N. Malhotra, 2004) and (Levine, 2007). A part of the image having 250 × 320 pixels of size within the rectangular area (Fig. 4) has been processed. We call this part the origin and show in Fig. 5.

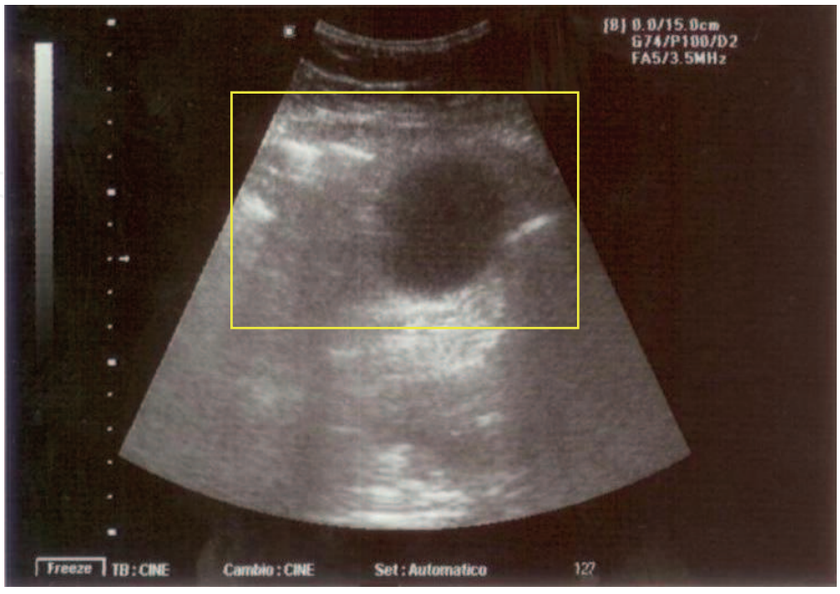

Fig. 4. The original ultrasound image.

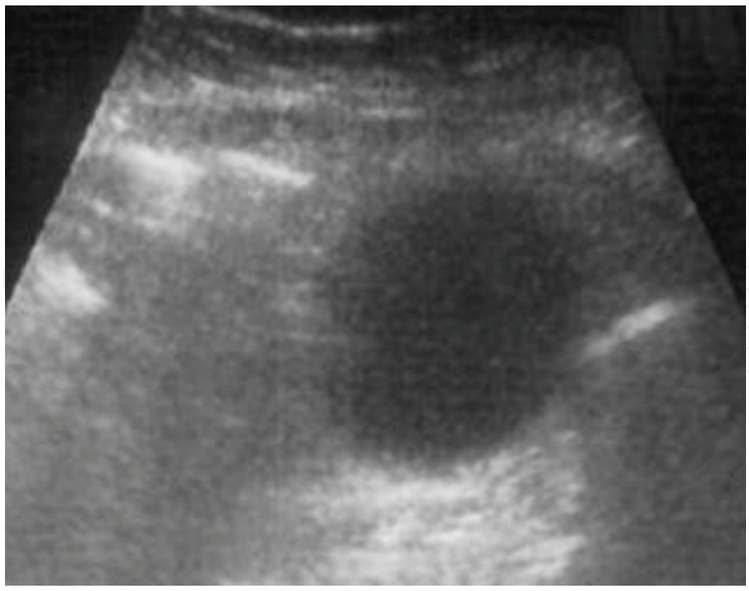

Fig. 5. A Section of the original ultrasound image of 250 × 320 pixels.

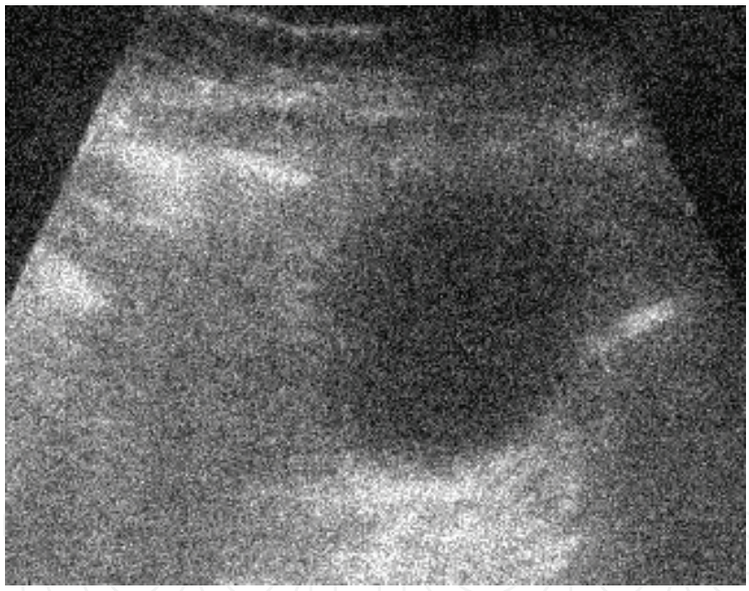

Fig. 6. A contaminated image (Fig. 5) with speckle noise and Gaussian noise, both having the variance $\sigma^2 = 0.01$.

The image was then intentionally contaminated with Gaussian noise and speckle noise, both having the variance $\sigma^2 = 0.01$, is shown in Fig. 6. To examine and exhibit an efficiency of the basic FIR FMH structure, we chose the following parameters: the number of points in the average, $N = 11$, the filter degree, $l = 1$, and the p parameter $p \in [-1, 1]$. The reader must be aware that determination of a certain set of the parameters is a special topic of optimization (minimizing both the SNR and the MSE) of the enhanced image.
Figure 7 shows us what is going on with the image if we let in the hybrid structure $p = 1$ (one-step predictive FIR filtering). In turn, Fig. 8 and Fig. 9 give us the pictures provided

with $p = 0$ (FIR filtering) and $p = -1$ (unit-leg smoothing FIR filtering). One can deduce that a visual comparison of Fig. 7—Fig. 9 does not reveal dramatic enhancements and a numerical analysis is in order. We apply such an analysis below postponing the results to several tables.

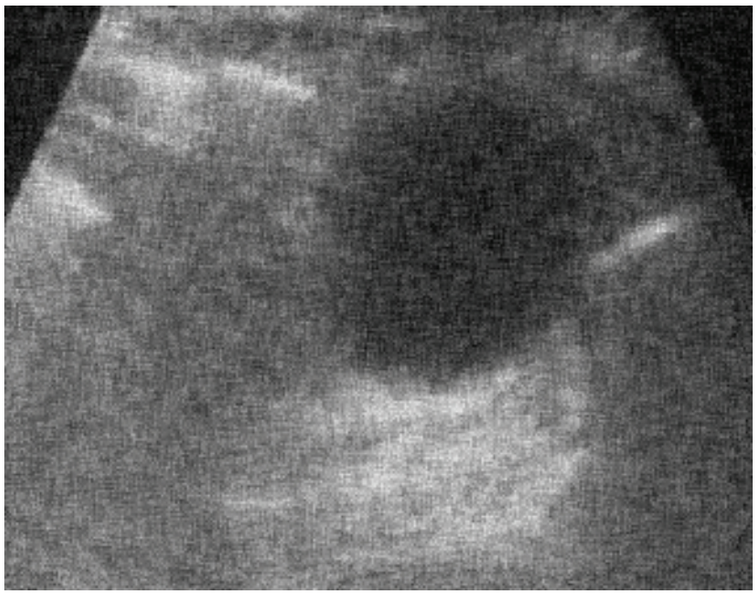

Fig. 7. An enhanced ultrasound image with $N = 11$, $l = 1$, and $p = 1$.

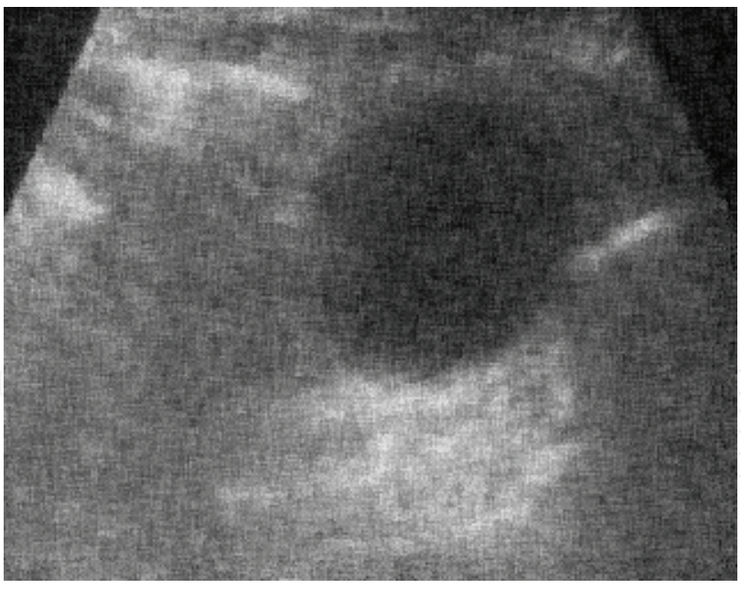

Fig. 8. An enhanced ultrasound image with $N = 11$, $l = 1$, and $p = 0$.

5.4 Analysis and discussions

In order to evaluate numerically the trade-off between the different filtering solutions employed in the FIR FMH structures, we use the SNR metric (83) and the RMSE metric (84) and apply them both to the reconstructed images obtained with different number k of sub-blocks, p-parameters, and degrees of the FIR filters, $l \in [0, 3]$, allowing $N = 11$.

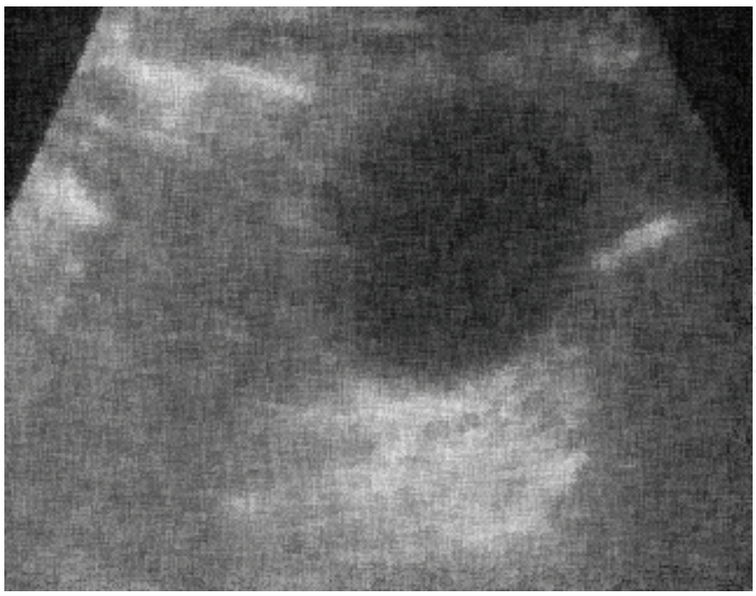

Fig. 9. An enhanced ultrasound image with $N = 11$, $l = 1$, and $p = -1$.

Fig. 10 and Fig. 11 show the RMSE and SNR as functions of p and Table 1 gives us several particular values of these measures. As can be seen, each of the degrees, $l \in [1, 3]$, allows obtaining both the maximum SNR and minimum RMSE. It is also seen that extremes of these functions are placed in the range of negative p. Specifically, it was revealed that the minimum errors are obtained with the $p = -1$ lag of the smoothing filter (Table 1). The latter speaks in favor of smoothing FIR filters for FMH structures, contrary to the predictive ones implemented in (Heinonen & Neuvo, 1987).

Effect of the FIR filter degree l on the RMSE and SNR is demonstrated in Table 2 for $p = -1$, $p = 0$, and $p = 1$. One can observe that the ramp filter ($l = 1$) produces minimum RMSEs and maximum SNRs in each of the cases, although the errors are minimum when $p = -1$. The quadratic gain ($l = 2$) and the cubic gain ($l = 3$) produce a bit worse results and simple averaging ($l = 0$) is not a rival with its large RMSE and small SNR. We thus infer that

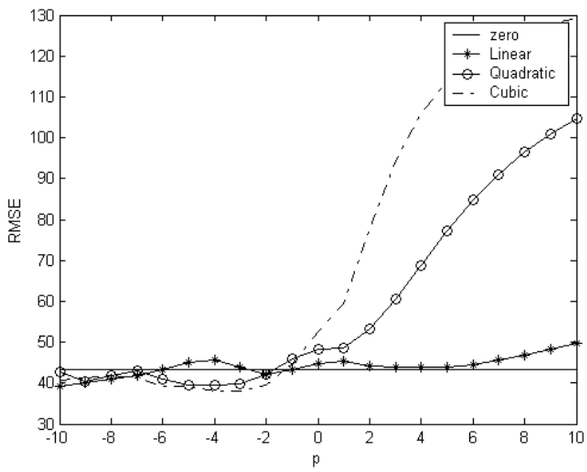

Fig. 10. RMSE in the enhanced image vs. p with $N = 11$, $k = 1$, $-5 \le p \le 5$, and $0 \le l \le 3$.

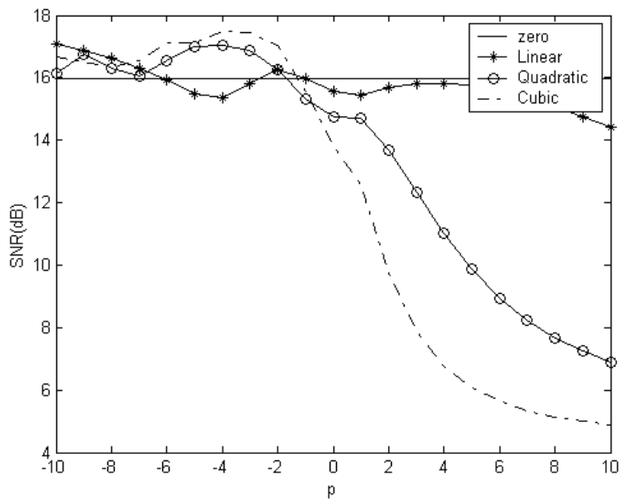

Fig. 11. SNR in the enhanced image vs. p with $N = 11$, $k = 1$, $-5 \le p \le 5$, and $0 \le l \le 3$.

	$p = -3$	$p = -2$	$p = -1$	$p = 0$	$p = 1$	$p = 2$	$p = 3$
RMSE	43.78	**42.24**	43.31	44.83	45.25	44.31	43.87
SNR (dB)	15.83	**16.24**	15.96	15.57	15.46	15.70	15.81

Table 1. Quantitative evaluation with $N = 11$, $k = 1$, and $l = 1$.

$p = -1$	$l = 0$	$l = 1$	$l = 2$	$l = 3$
RMSE	**43.24**	43.31	45.87	44.88
SNR, dB	**15.97**	15.96	15.31	15.55

$p = 0$	$l = 0$	$l = 1$	$l = 2$	$l = 3$
RMSE	**43.24**	44.83	48.33	52.63
SNR, dB	15.97	**15.57**	14.74	13.81

$p = 1$	$l = 0$	$l = 1$	$l = 2$	$l = 3$
RMSE	**43.24**	45.25	48.49	59.27
SNR, dB	**15.97**	15.46	14.70	12.56

Table 2. Quantitative evaluation with $N = 11$, $k = 1$, and $p \in [-1, 1]$.

complex FIR FMH structures need to be optimized in the sense of the minimum RMSE over l and p simultaneously and that there is an optimal solution behind each of such structures.

The next important point for the optimization is the k of the sub-blocks. At a first glance, every new sub-block should reduce errors in the median filter, because the latter acquires more entries to make a decision. Indeed, in our experiment illustrated in Fig. 12 and Fig. 13 this deduction has not been confirmed: an increase in k from 1 to 3 results in these figures in the RMSE reduction and increasing the SNR. Table 3 gives us extreme points of these functions in the p-domain.

Effect of noise on the RMSE and SNR in the enhanced image has been investigated by changing the noise variance. Fig. 14 and Fig. 15 give an idea about such an influence. First, we arrive at an almost self-obvious conclusion that the RMSE rises and the SNR diminishes

when the noise variance increases. That is neatly seen in Fig. 14 and Fig. 15. What has appeared to be lesser expected is that the RMSE minimum and the SNR maximum both remove to the range of larger p since the variance increases. In fact, we watch in Fig. 14 for the RMSE minimum at p = -1 with σ^2 = 0.02 and at p = 1 with σ^2 = 0.08. Certainly this effect needs more investigations as being affecting the optimal set of parameters.

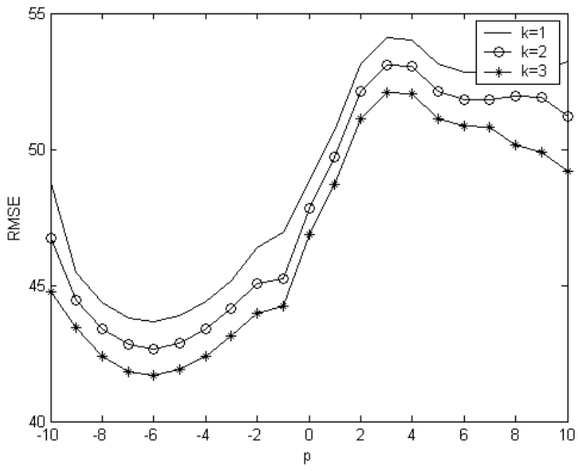

Fig. 12. RMSE in the enhanced image vs. p with N = 11, l = 1, – 5 ≤ p ≤ 5, and 1 ≤ k ≤ 3.

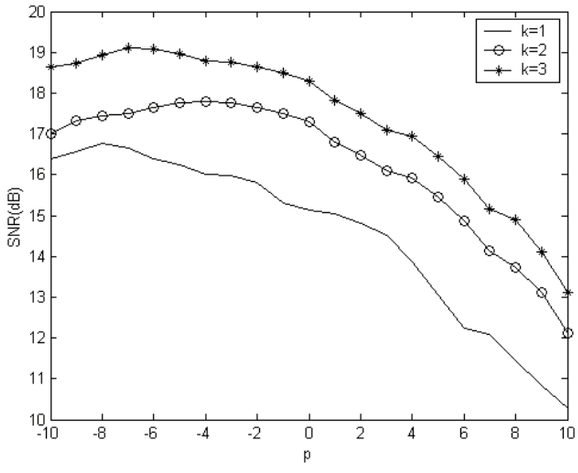

Fig. 13. Sketches of SNR vs. p with N = 11, l = 1, – 5 ≤ p ≤ 5, 1 ≤ k ≤ 3.

	k = 1	k = 2	k = 3
$RMSE_{min}$	15.13	17.29	**18.27**
SNR_{max} (dB)	48.85	47.74	**46.63**

Table 3. Quantitative evaluation with N = 11, l = 1, and p = –1.

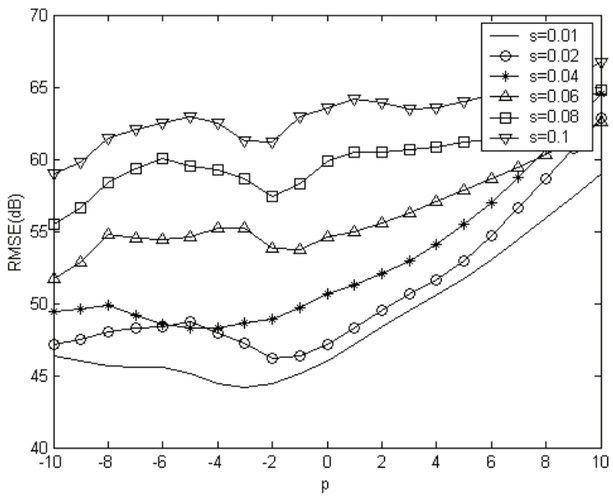

Fig. 14. RMSE vs. p with $N = 11$, $l = 1$, $k = 1$, $-5 \le p \le 5$, and $0.01 \le \sigma^2 \le 0.1$.

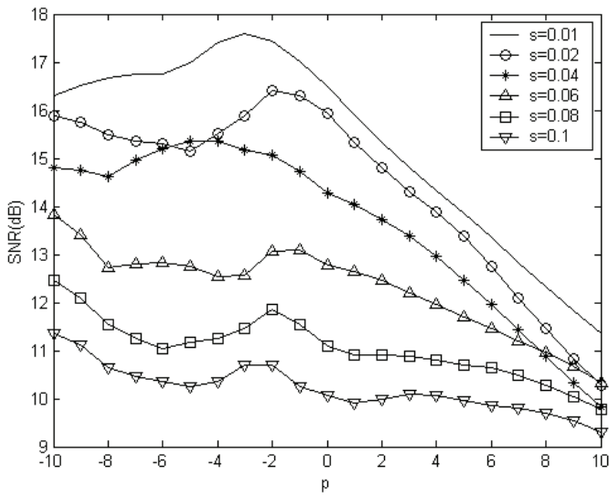

Fig. 15. SNR vs. p with $N = 11$, $l = 1$, $k = 1$, $-5 \le p \le 5$, and $0.01 \le \sigma^2 \le 0.1$.

6. Conclusion

In this chapter, we developed the theory of smoothing FIR filtering and applied the results to the design of FIR median hybrid filters in order to enhance ultrasound images. General smoothing filter gain has been derived in line with the most widely used low-order ones. We propose an unbiased solution. The gain for the unbiased smoother had been developed in the unique polynomial form that does not involve any knowledge about noise and initial state, thus having strong engineering features. It has been shown experimentally that, as a rule of thumb, the smoothing FIR filters with $p < 0$ allow for lower RMSEs and larger SNRs in the enhanced image. On the other hand, our experiments reveal that predictive filtering solutions earlier used in (Heinonen & Neuvo, 1987) in ultrasound image processing (Morales-Mendoza et. al, 2008, 2009) produce large errors.

7. References

K. Najarian and R. Splinter, *Biomedical Signal and Image Processing*. New York: CRC Taylor & Francis, 2007.

J. Jan, *Medical Image Processing, Reconstruction and Restoration: Concept and Methods*. Florida USA: CRC Taylor & Francis Press, 2006.

I. Pitas and A. Venetsanopoulos, *Nonlinear Digital Filters – Principles and Applications*, Kluwer Academic Publishers, 1990.

N. Kalouptsidis and S. Theodoridis, *Adaptive system Identification and signal processing Algorithms*, Prentice Hall, 1993.

J. Astola and P. Kuosmanen, *Fundamentals of Nonlinear Digital Filters*, CRC Press, 1997.

P. Heinonen and A. Neuvo, FIR median hybrid filters, *IEEE Trans. on Acoustic, Speech, and Signal Processing*, vol. 35, no. 6, pp. 832-838, June 1987.

P. Heinonen and A. Neuvo, FIR-median hybrid filter with predictive FIR substructures, *IEEE Trans. on Acoustic, Speech, and Signal Processing*, vol. 36, no. 6, pp. 892-899, June 1988.

Dumitrescu; B. *Positive Trigonometric Polynomials and Signal Processing Applications*, Springer, Dordrecht, ISBN 978-1402051241, 2007.

Mathews; V. J. & Sicuranza ; G. L. *Polynomials Signal Processing*, John Wiley & Sons, New York, ISBN 978-0471034148, 2001.

Y. Shmaliy, An unbiased FIR filter for TIE model of a local clock in applications to GPS-based timekeeping, *IEEE Trans. on Ultrasonic, Ferroelectrics and Frequency Control*, vol. 53, no. 5, pp. 862-870, May 2006.

T. Bose, F. Meyer, and M.-Q. Chen, *Digital Signal and Image Processing,* J. Wiley, New York, 2004

Y. Shmaliy, An unbiased *p*-step predictive FIR filter for a class of noise-free discrete time models with independently observed states, *Signal, Image & Video Processing,* vol. 3, no. 2, pp. 127-135, Jun. 2009.

Y. Shmaliy, Optimal gains of FIR estimators for a class of discrete-time state-space models, *IEEE Signal Processing Letters,* vol. 15, pp. 517-520, 2008.

Y. Shmaliy, Unbiased FIR filtering of discrete-time polynomial state-space models, *IEEE Transactions on Signal Processing,* vol. 57, no. 4, pp. 1241-1249, Apr. 2009.

S. W. Smith, *The Scinetist and Engineer's Guide to Digital Signal Processing*, 2nd Ed., California Technical Publishing, 1999.

D. Levine, *Ultrasound Clinics*, ELSEVIER INC., Boston USA, 2007.

K. Singh & N. Malhotra, *Step-by-Step Ultrasound in Obstetrics*, Mc-Graw Hill, 2004.

L. J. Morales-Mendoza, Y. Shmaliy, O. G. Ibarra-Manzano, L. J. Arceo-Miquel and M. Montiel-Rodriguez, Moving Average Hybrid FIR Filter in Ultrasound Image Processing, *Proceeding of 18th International Conference of CONIELECOMP*, ISBN: 0-7695-3120-2, pp. 160 – 164, Cholula, Pue. Mexico, March 2008.

L. J. Morales-Mendoza, Y. Shmaliy and O. G. Ibarra-Manzano, An analysis of Hybrid FIR Structures in application to Ultrasound Image Processing, *Proceeding of 1st International Conference of WSEAS*, ISBN: 978-960-474-071-0, pp. 344-349, Houston Tx, USA, May 2009.

Image Processing

Edited by Yung-Sheng Chen

ISBN 978-953-307-026-1

Hard cover, 516 pages

Publisher InTech

Published online 01, December, 2009

Published in print edition December, 2009

There are six sections in this book. The first section presents basic image processing techniques, such as image acquisition, storage, retrieval, transformation, filtering, and parallel computing. Then, some applications, such as road sign recognition, air quality monitoring, remote sensed image analysis, and diagnosis of industrial parts are considered. Subsequently, the application of image processing for the special eye examination and a newly three-dimensional digital camera are introduced. On the other hand, the section of medical imaging will show the applications of nuclear imaging, ultrasound imaging, and biology. The section of neural fuzzy presents the topics of image recognition, self-learning, image restoration, as well as evolutionary. The final section will show how to implement the hardware design based on the SoC or FPGA to accelerate image processing.

InTech Europe

University Campus STeP Ri
Slavka Krautzeka 83/A
51000 Rijeka, Croatia
Phone: +385 (51) 770 447
Fax: +385 (51) 686 166
www.intechopen.com

InTech China

Unit 405, Office Block, Hotel Equatorial Shanghai
No.65, Yan An Road (West), Shanghai, 200040, China
中国上海市延安西路65号上海国际贵都大饭店办公楼405单元
Phone: +86-21-62489820
Fax: +86-21-62489821

IntechOpen